International Journal of Solids and Structures 45 (2008) 5015–5034

Contents lists available at ScienceDirect

International Journal of Solids and Structures

journal homepage: www.elsevier.com/locate/ijsolstr

Response of railway track system on poroelastic half-space soil medium subjected to a moving train load

Yuanqiang Cai [a,b], Honglei Sun [a], Changjie Xu [a,*]

[a] MOE Key Laboratory of Soft Soils and Geoenvironmental Engineering, Zhejiang University, Zhejiang, Hangzhou 310027, PR China
[b] College of Architecture and Civil Engineering, Wenzhou University, Wenzhou 325035, PR China

ARTICLE INFO

Article history:
Received 25 April 2007
Received in revised form 19 February 2008
Available online 11 May 2008

Keywords:
Poroelasticity
Railroad tracks
Railroad trains
Soil dynamics
Fourier transform

ABSTRACT

Based on the dynamic poroelastic theory of Biot, dynamic responses of a track system and poroelastic half-space soil medium subjected to moving train passages are investigated by the substructure method. The whole system is divided into two separately formulated substructures, the track and the ground, and the rail is described by introducing the Green function for an infinitely long Euler beam subjected to the action of moving axle loads of the train and the reactions of the sleeper. Sleepers are represented by a continuous mass and the effect of the ballast is considered by introducing the Cosserat model for granular medium. Using the double Fourier transform, the governing equations of motion are then solved analytically in the frequency-wave-number domain. The time domain responses are evaluated by the inverse Fourier transform computation for a certain train speed. Computed results show that the shape of the rail displacements of the elastic and poroelastic soil medium are in good agreement with each other of the low train velocity, but the result of the poroelastic soil medium is significantly different to that of the elastic soil medium for the high train velocity which is higher than Rayleigh-wave speed in the soil. The influence of the soil intrinsic permeability on soil responses is discussed with great care in both time domain and frequency domain. The dynamic responses of the soil medium are considerably affected by the fluid phase as well as the load velocity.

1. Introduction

Studies of the dynamic response of railway track and adjoining ground under the action of moving train has received considerable attention in a number of engineering fields such as civil engineering, transportation engineering and environmental engineering. Recently high-speed trains are becoming increasingly popular and freight trains becoming heavier. Combined with this finding and the observation that Rayleigh-wave speeds are slow in soft soils, it can be seen that the study of the dynamic response subjected to moving train load is important for environmental sense of the along side built-in area.

Vibration of a track system on the ground was first considered by Kennedy and Herrmann (1973a,b) who gave an analytical solution a visco-elastic ground under moving point load. From then on, many soil models are represented to predict the wave propagation in the track-ground system under the moving load. Kargarnovin et al. (2005) and Kargarnovin and Younesian (2004) investigated the response of a Timshenko beam on the Pasternak visco-elastic half-space and nonlinear visco-elastic half-space respectively. Sheng et al. (1999), Takemiya and Bian (2005) and Picoux and Le Houedec (2005) extended the investigations to the more realistic layered ground system. Kim (2004, 2006) successively analyzed the track-

* Corresponding author. Tel./fax: +86 571 8795 2619.
E-mail address: changjie.xu@gmail.com (C. Xu).

0020-7683/$ - see front matter © 2008 Elsevier Ltd. All rights reserved.
doi:10.1016/j.ijsolstr.2008.05.002

ground system considering the ground as a Winkler-type or a two-parameter foundation and the linear hysteretic damping was taken into account. Generally, there is under-ground water in the considered soil medium, and the existence of the water affects the wave propagation in the soil medium in some degree during the passage of the train. The fully saturated poroelastic soil model superior to the linear or visco-elastic one is a good choice to be used for the analysis of dynamic responses of the track-ground system.

There are many researchers deal with dynamic responses of a fully saturated soil under moving load. Burke and Kingsbury (1984) presented an analytical solution for a poroelastic medium subjected to traveling surface pressure. Siddharthan et al. (1993) presented works on the dynamic response of a poroelastic half-space to moving load under plane strain condition. The couple of soil and fluid was neglected in the works. Theodorakopoulos (2003) and Theodorakopoulos et al. (2004) considering the relative motion between solid and fluid on the basis of Siddharthan et al. (1993), studied the response of a poroelastic half-plane soil medium subjected to moving loads analytically/numerically. Jin et al. (2004) studied the responses of a poroelastic half-space subjected to a moving point load under plane strain condition. The steady state responses of a fully saturated poroelastic half-space subjected to a moving rectangular load was investigated by Cai et al. (2007), the track system was not considered in the work. It is noted that although many problems involving consolidation or dynamic response of poroelastic media have been considered, the study dealt with the application of Biot's theory for analysis of dynamic responses of railway track system on poroelastic half-space under moving train load are rather limited. Most of the existing works did not concern three dimensional models, the railway track system, and practical train load. Two dimensional models are not able to reproduce mechanisms of wave propagation in the poroelastic half-space correctly since the loading zone represents a reduced area compared to infinite ground surface, thus excluding the hypothesis of plane deformation. The railway track system influenced the dynamic responses as widely known, and a practical train load is superior to both point load and line load.

In this paper, based on the dynamic poroelastic theory of Biot, an analytical model for the track-ground system taking into account the coupling of soil particles and pore water of the soil medium is presented. The rail is described by introducing the Green function for an infinitely long Euler beam subjected to the action of the moving axle loads of the train and reactions of the sleeper. Sleepers are represented by a continuous mass and the effect of the ballast is considered. The full dynamic poroelastic theory of Biot was employed. Using the double Fourier transform, the governing equations of motion are then solved analytically in the frequency-wave-number domain. The time domain responses are evaluated by the inverse Fourier transform computation for a certain train speed. The influence of the soil intrinsic permeability on soil responses is systematically discussed in both time domain and frequency domain under low and high train velocity.

2. Governing equations and general solutions

2.1. Analytical solution of poroelastic half-space

The system considered herein, shown in Fig. 1, consists of a uniform porous elastic solid material, fully saturated by a viscous fluid, and extended to infinity in x, y, z directions. The fluid is free to flow throughout the entire upper surface. The rail is described by introducing the Green function for an infinite long Euler beam subjected to the action of the moving axle loads of the train and the reactions of the sleeper. Sleepers are represented by a continuous mass and the effect of the ballast is considered by introducing the Cosserat model for granular medium.

Based on the assumption of neglecting the apparent mass density, the linearized dynamic equations of motion of fully saturated poroelastic is given as Biot (1956):

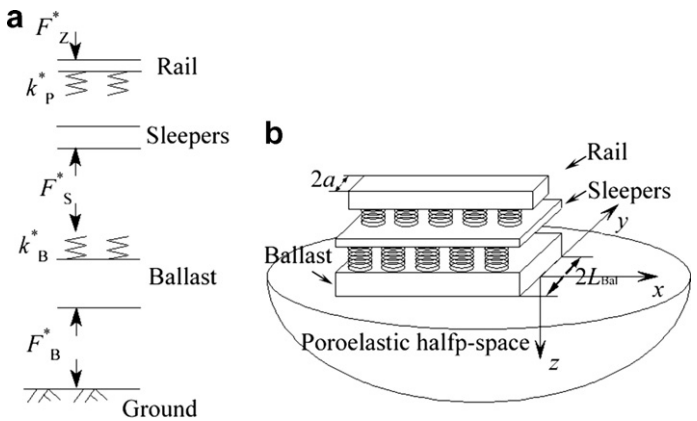

Fig. 1. Coupled track-ground model with sleepers: (a) the details of the model and (b) the main model.

$$\mu u_{i,jj} + (\lambda + \alpha^2 M + \mu) u_{j,ji} + \alpha M w_{j,ji} = \rho \ddot{u}_i + \rho_f \ddot{w}_i \tag{1}$$

$$\alpha M u_{j,ji} + M w_{j,ji} = \rho_f \ddot{u}_i + m \ddot{w}_i + b \dot{w}_i \tag{2}$$

where, u_i, w_i ($i = x, y, z$) are the solid displacement components and fluid displacement related to solid displacement along the x, y, z directions; the subscript $_{i,jj}$, $_{j,ji}$ are symbols of tensor; dots on u_i and w_i indicate the differential with respect to time t; λ and μ are Lame constants; α and M are Biot's parameters accounting for compressibility of the two-phased material; ρ and ρ_f are the actual mass densities of the solid and the fluid, respectively; m is a density-like parameter that depends on ρ_f and the geometry of the pores; b is a parameter accounting for the internal friction due to the relative motion between the solid and the pore fluid. The parameter b equals to the ratio between the fluid viscosity and the intrinsic permeability of the medium ($b = 0$ for the neglection of internal friction). The constitutive relations can be expressed as:

$$\sigma_{ij} = \lambda \delta_{ij} \theta + \mu (u_{i,j} + u_{j,i}) - \alpha \delta_{ij} p \tag{3}$$

$$p = -\alpha M \theta + M \varsigma \tag{4}$$

where

$$\varsigma = -w_{i,i} \tag{5}$$

and $\theta = u_{i,i}$ is solid strain; σ_{ij} is the total stress component of bulk material; p is the pore water pressure.

In this paper, the dimensionless coordinates are defined as: $x^* = x/a$, $y^* = y/a$, $z^* = z/a$ and the dimensionless time is defined as $\tau = (t/a)\sqrt{\mu/\rho}$, in which a is the half width of the railway track.

The Fourier transform with respect to dimensionless time τ is defined as

$$\tilde{f}(x^*, y^*, z^*, \Omega) = \int_{-\infty}^{\infty} f(x^*, y^*, z^*, \tau) e^{-i\Omega\tau} d\tau \tag{6}$$

and the inverse relationship is given by

$$f(x^*, y^*, z^*, \tau) = \frac{1}{2\pi} \int_{-\infty}^{\infty} \tilde{f}(x^*, y^*, z^*, \Omega) e^{i\Omega\tau} d\Omega \tag{7}$$

By making use of Eq. (6) and after some manipulations, Eqs. (1)–(5) lead to the following form:

$$\nabla^2 \tilde{u}_x + (\lambda^* + 1) \frac{\partial \tilde{\theta}}{\partial x^*} + \Omega^2 (1 - \rho^* \vartheta) \tilde{u}_x - (\alpha - \vartheta) \frac{\partial \tilde{p}}{\partial x^*} = 0 \tag{8}$$

$$\nabla^2 \tilde{u}_y + (\lambda^* + 1) \frac{\partial \tilde{\theta}}{\partial y^*} + \Omega^2 (1 - \rho^* \vartheta) \tilde{u}_y - (\alpha - \vartheta) \frac{\partial \tilde{p}}{\partial y^*} = 0 \tag{9}$$

$$\nabla^2 \tilde{u}_z + (\lambda^* + 1) \frac{\partial \tilde{\theta}}{\partial z^*} + \Omega^2 (1 - \rho^* \vartheta) \tilde{u}_z - (\alpha - \vartheta) \frac{\partial \tilde{p}}{\partial z^*} = 0 \tag{10}$$

$$\nabla^2 \tilde{p} + \frac{\rho^* \Omega^2}{M^* \vartheta} \tilde{p} + \frac{\rho^* \Omega^2 (\alpha - \vartheta)}{\vartheta} \tilde{\theta} = 0 \tag{11}$$

The dimensionless parameters in the former equations are defined as: $\lambda^* = \lambda/\mu$, $M^* = M/\mu$, $\rho^* = \rho_f/\rho$, $m^* = m/\rho$, $b^* = ab/\sqrt{\rho\mu}$, $\vartheta = \rho^* \Omega^2/(m^* \Omega^2 - i b^* \Omega)$ and ∇^2 is the Laplacian operator defined by

$$\nabla^2 = \frac{\partial^2}{\partial x^{*2}} + \frac{\partial^2}{\partial y^{*2}} + \frac{\partial^2}{\partial z^{*2}}$$

From Eqs. (8)–(11) the following equation can be obtained:

$$\nabla^4 \tilde{p} + a_1 \nabla^2 \tilde{p} + a_2 \tilde{p} = 0 \tag{12}$$

in which

$$a_1 = \frac{(m^* \Omega^2 - i b^* \Omega)(\lambda^* + \alpha^2 M^* + 2) + M^* \Omega^2 - 2\alpha M^* \rho^* \Omega^2}{(\lambda^* + 2) M^*} \tag{13}$$

$$a_2 = \frac{(m^* \Omega^2 - i b^* \Omega) \Omega^2 - (\rho^*)^2 \Omega^4}{(\lambda^* + 2) M^*} \tag{14}$$

The Fourier transforms with respect to the dimensionless x-coordinate and y-coordinate is defined as

$$\bar{\tilde{f}}(\xi, \eta, z^*, \Omega) = \int_{-\infty}^{\infty} \int_{-\infty}^{\infty} f(x^*, y^*, z^*, \Omega) e^{-i(\xi x^* + \eta y^*)} dx^* dy^* \tag{15}$$

and the inverse relationship is given by

$$f(x^*,y^*,z^*,\Omega)=\frac{1}{4\pi^2}\int_{-\infty}^{\infty}\int_{-\infty}^{\infty}\bar{\bar{f}}(\xi,\eta,z^*,\Omega)\mathrm{e}^{\mathrm{i}(\xi x^*+\eta y^*)}\mathrm{d}\xi\mathrm{d}\eta \tag{16}$$

The application of Fourier integral transforms to Eqs. (3), (4) and (8)–(11) leads to

$$\bar{\bar{p}}(\xi,\eta,z^*,\Omega)=A(\xi,\eta,\Omega)\mathrm{e}^{-\gamma_1 z^*}+B(\xi,\eta,\Omega)\mathrm{e}^{-\gamma_2 z^*} \tag{17}$$

$$\bar{\bar{u}}_z(\xi,\eta,z^*,\Omega)=\gamma_1 F_1 A(\xi,\eta,\Omega)\mathrm{e}^{-\gamma_1 z^*}+\gamma_2 F_2 B(\xi,\eta,\Omega)\mathrm{e}^{-\gamma_2 z^*}+C(\xi,\eta,\Omega)\mathrm{e}^{-\gamma_3 z^*} \tag{18}$$

$$\bar{\bar{u}}_y(\xi,\eta,z^*,\Omega)=-\mathrm{i}\eta[F_1 A(\xi,\eta,\Omega)\mathrm{e}^{-\gamma_1 z^*}+F_2 B(\xi,\eta,\Omega)\mathrm{e}^{-\gamma_2 z^*}]+\mathrm{i}D(\xi,\eta,\Omega)\mathrm{e}^{-\gamma_3 z^*} \tag{19}$$

$$\bar{\bar{u}}_x(\xi,\eta,z^*,\Omega)=-\frac{\mathrm{i}}{\xi}\{[E_1+(\xi^2-b_1^2)F_1]A\mathrm{e}^{-\gamma_1 z^*}+[E_2+(\xi^2-b_2^2)F_2]B\mathrm{e}^{-\gamma_2 z^*}+(C\gamma_3+D\eta)\mathrm{e}^{-\gamma_3 z^*}\} \tag{20}$$

in which

$$\gamma_i=\sqrt{\xi^2+\eta^2-b_i^2},\quad i=1,2$$

$$\gamma_3=\sqrt{\xi^2+\eta^2+D^2}$$

$$E_i=\frac{\vartheta M^* b_i^2-\rho^*\Omega^2}{\rho^*\Omega^2(\alpha-\vartheta)M^*},\quad i=1,2$$

$$F_i=\frac{\lambda^* E_i+E_i-\alpha+\vartheta}{D^2-b_i^2},\quad i=1,2$$

$$b_1^2=\frac{a_1+\sqrt{a_1^2-4a_2}}{2},\quad b_2^2=\frac{a_1-\sqrt{a_1^2-4a_2}}{2}$$

$$D^2=(1-\rho^*\vartheta)\Omega^2$$

As the model studied concerns half-space problem, the real part of γ_i (i = 1, 2, 3) must be positive to fulfill the infinite boundary conditions of the half-space.

Boundary conditions of the half-space are given as follows:

$$\sigma_{zz}(x^*,y^*,0,\tau)=-\frac{1}{2a}\Pi(y^*)q_z(x^*,\tau) \tag{21}$$

$$\tau_{xz}(x^*,y^*,0,\tau)=0 \tag{22}$$

$$\tau_{yz}(x^*,y^*,0,\tau)=0 \tag{23}$$

$$p(x^*,y^*,0,\tau)=0 \tag{24}$$

$$\Pi(y^*)u_z(x^*,0,0,\tau)=u_{\mathrm{B}}(x^*,\tau) \tag{25}$$

where $q_z(x^*,\tau)$ is the ballast force on the ground; $u_{\mathrm{B}}(x^*,\tau)$ denotes the ballast displacement at the surface of the ground and Eq. (25) indicates that the displacement of the surface of the ground under the ballast is equal to the displacement of the ballast. And the load distributing function is defined as

$$\Pi(y^*)=\begin{cases}1 & |y^*|\leqslant L_{\mathrm{Bal}}^*\\ 0 & |y^*|>L_{\mathrm{Bal}}^*\end{cases} \tag{26}$$

in which, L_{Bal} is the half ballast width, and $L_{\mathrm{Bal}}^*=L_{\mathrm{Bal}}/a$ denotes the dimensionless half ballast width.

Using expressions of Eqs. (3) and (4), the Fourier transformed of u_z under the boundary conditions of Eqs. (21)–(24) are given as follows:

$$\bar{\bar{u}}_z(\xi,\eta,z^*,\Omega)=-\overline{\Pi}(\eta)\bar{\bar{q}}_z(\xi,\Omega)\phi(\xi,\eta,z^*,\Omega) \tag{27}$$

where

$$\phi(\xi,\eta,z^*,\Omega)=\frac{1}{\Delta}[(\gamma_3^2+\xi^2+\eta^2)(\gamma_2 a_2\mathrm{e}^{-\gamma_2 z^*}-\gamma_1 a_1\mathrm{e}^{-\gamma_1 z^*})+(\gamma_1 g_5-\gamma_2 g_6)\mathrm{e}^{-\gamma_3 z^*}]$$

$$g_i=E_i+(2\xi^2-b_i^2)F_i,\quad i=1,2$$

$$g_3=\lambda^* E_1-2\gamma_1^2 F_1-\alpha,\quad g_4=\lambda^* E_2-2\gamma_2^2 F_2-\alpha$$

$$g_5=g_1+2\eta^2 a_1,\quad g_6=g_2+2\eta^2 a_2$$

$$\Delta=(g_4-g_3)(\gamma_3^2+\xi^2+\eta^2)-2\gamma_3(\gamma_1 g_5-\gamma_2 g_6)$$

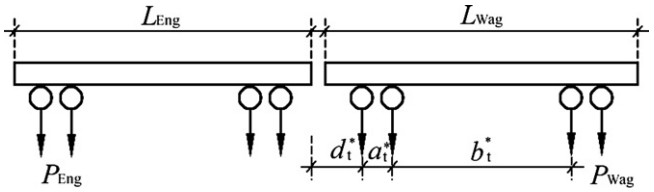

Fig. 2. Representation of train excitation.

2.2. Description of the railway track

The track system used here is introduced from that of Picoux and Le Houedec (2005). The dimensionless equation for the rails represented by an Euler Beam is written as

$$\delta\frac{\partial^4 u_R(x^*,\tau)}{\partial x^{*4}}+m_R^*\frac{\partial^2 u_R}{\partial\tau^2}+k_P^*[u_R(x^*,\tau)-u_S(x^*,\tau)]=\begin{cases}F_z^*(x^*,\tau) & x^*-c^*\tau=0\\ 0 & x^*-c^*\tau\neq 0\end{cases} \tag{28}$$

in which u_R is the displacement of the Euler beam, $\delta = EI/\mu a^4$ is the dimensionless bending rigidity of the rail, $m_R^* = m_R/\rho a^2$ is the dimensionless mass of the rail per unit length, $k_P^* = k_P/\mu a$ denotes the dimensionless spring constant of the rail pads, $F_z^* = F_z/\mu a^2$ is the dimensionless load acting on the Euler beam, u_S is the displacement of the sleepers, $c^* = V\sqrt{\rho/\mu}$ is the dimensionless load velocity and $x^* - c^*\tau$ indicates the load position.

It is shown by Vostroukhov and Metrikine (2003) that the vertical displacement due to train passage over a track with discrete sleeper positions is almost identical to the results when the sleepers are uniformly distributed along the track. Hence sleepers are represented by a continuous mass in the dimensionless equation as

$$m_S^*\frac{\partial^2 u_S(x^*,\tau)}{\partial\tau^2}+k_P^*[u_S(x^*,\tau)-u_R(x^*,\tau)]=-F_S^*(x^*,\tau) \tag{29}$$

where $m_S^* = m_S/\rho a^2$ is the dimensionless mass of the sleepers per unit length, $F_S^* = F_S/\mu a^2$ is the dimensionless force between the sleepers and the ballast.

The ballast is first considered by Cosserat model by Suiker et al. (1999). At the top and bottom of the ballast, the system is written as (dimensionless):

Table 1
Parameters of a train

P_{Eng}^*	0.008
P_{Wag}^*	0.005
L_{Eng}^*	22.2
L_{Wag}^*	24.4
a_t^*	2.9
b_t^*	14.8
d_t^*	4
L_{Dis}^*	−35

Table 2
Dimensionless parameters of a rail-track and soil

Dimensionless coefficients	Numerical values
Lame constants, λ^*	2
Compressibility of water, M^*	12
Water density, ρ^*	0.53
Hysteretic damping ratio, β	0.02
Parameter of soil structure, m^*	1.5625
Compressibility of soil grain, α	0.97
Ratio between fluid viscosity and permeability, b^*	10
Beam bending rigidity, δ	1
Beam mass of unit length, m_R^*	2
Spring constant, $k_P^* = k_B^*$	2.7
Sleeper mass of unit length, m_S^*	4
Ballast mass of unit length, m_B^*	10
Half width of the Ballast, L_{Bal}^*	2

$$\frac{m_B^*}{6}\left[2\frac{\partial^2 u_S(x^*,\tau)}{\partial\tau^2}+\frac{\partial^2 u_B(x^*,\tau)}{\partial\tau^2}\right]+k_B^*[u_S(x^*,\tau)-u_B(x^*,\tau)]=F_S^*(x^*,\tau) \tag{30}$$

$$\frac{m_B^*}{6}\left[\frac{\partial^2 u_S(x^*,\tau)}{\partial\tau^2}+2\frac{\partial^2 u_B(x^*,\tau)}{\partial\tau^2}\right]+k_B^*[-u_S(x^*,\tau)+u_B(x^*,\tau)]=-F_B^*(x^*,\tau) \tag{31}$$

in which $m_B^*=m_B/\rho a^2$ is the dimensionless mass of the ballast per unit length, $k_B^*=k_B/\mu a^2$ is the dimensionless spring constant between ballast and sleepers and $F_B^*=F_B/\mu a^2$ is the dimensionless ballast force on the soil. F_B^* equals $q_z(x^*,\tau)$ in Eq. (21).

Using Eqs. (6) and (15), the following set of equations relative to the track in Fourier transformed domain is obtained from Eqs. (27)–(31) after eliminating F_S^*:

$$\begin{cases}\alpha_1(\xi,\Omega)\tilde{\bar{u}}_R(\xi,\Omega)-k_p^*\tilde{\bar{u}}_S(\xi,\Omega)=\alpha_2(\xi,\Omega)\\ -k_p^*\tilde{\bar{u}}_R(\xi,\Omega)+\alpha_3(\xi,\Omega)\tilde{\bar{u}}_S(\xi,\Omega)+\alpha_4(\xi,\Omega)\tilde{\bar{u}}_B(\xi,\Omega)=0\\ \alpha_4(\xi,\Omega)\tilde{\bar{u}}_S(\xi,\Omega)+\alpha_5(\xi,\Omega)\tilde{\bar{u}}_B(\xi,\Omega)=-\tilde{\bar{F}}_B^*(\xi,\Omega)\\ \tilde{\bar{u}}_B(\xi,\Omega)=\alpha_6(\xi,\Omega)\tilde{\bar{F}}_B^*(\xi,\Omega)\end{cases} \tag{32}$$

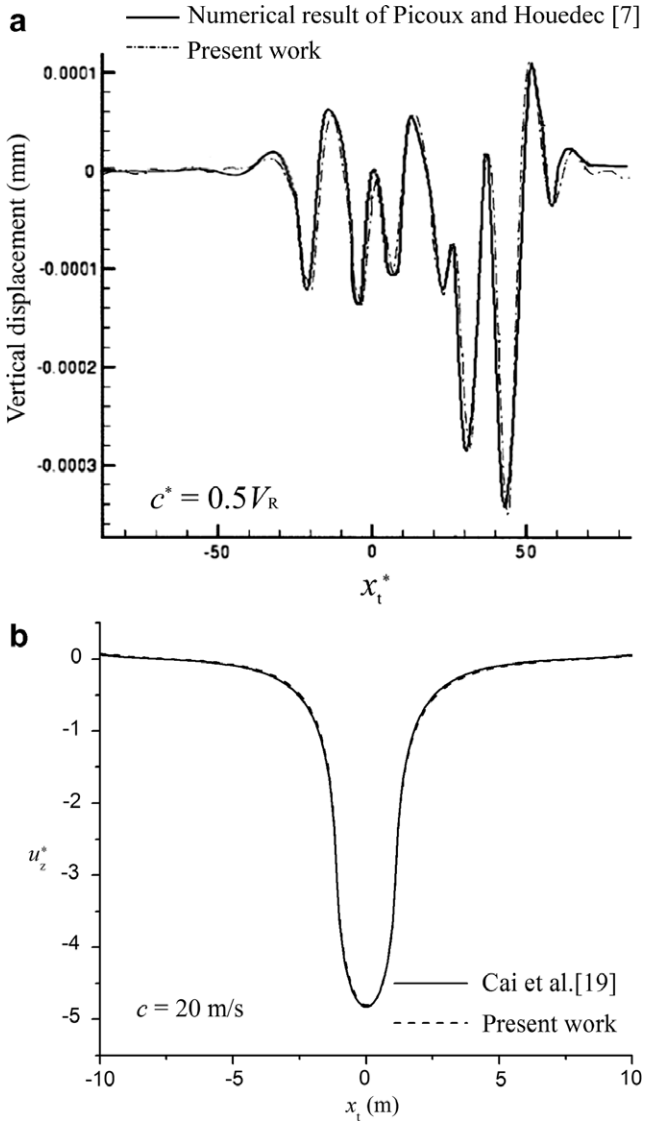

Fig. 3. Comparison with the existing work: (a) with that of Picoux and Le Houedec (2005); (b) with that of Cai et al. (2007).

where

$$\alpha_1(\xi,\Omega) = \delta\xi^4 - m_R^*\Omega^2 + k_P^*$$
$$\alpha_2(\xi,\Omega) = F_z^*(\xi,\Omega)$$
$$\alpha_3(\xi,\Omega) = -m_B^*\Omega^2/2 + k_P^* + k_B^* - m_S^*\Omega^2$$
$$\alpha_4(\xi,\Omega) = -m_B^*\Omega^2/6 - k_B^*$$
$$\alpha_5(\xi,\Omega) = -m_B^*\Omega^2/3 + k_B^*$$
$$\alpha_6(\xi,\Omega) = \Psi(\xi,0,\Omega)$$
$$\Psi(\xi,0,\Omega) = \frac{1}{2\pi}\int_{-\infty}^{\infty} -\overline{\Pi}^2(\eta)\phi(\xi,\eta,0,\Omega)e^{i\eta y}dy$$

Solution of Eq. (32) yields the force expression:

$$\overline{\overline{F}}_B^*(\xi,\Omega) = \frac{\alpha_2(\xi,\Omega)\alpha_4(\xi,\Omega)k_P^*}{\alpha_1(\xi,\Omega)\alpha_6(\xi,\Omega)\alpha_4^2(\xi,\Omega) - (\alpha_3(\xi,\Omega)\alpha_1(\xi,\Omega) - k_P^{*2})(1+\alpha_5(\xi,\Omega)\alpha_6(\xi,\Omega))} \tag{33}$$

and soil displacement in Fourier transform domain is finally given by

$$\overline{\overline{\overline{u}}}_z(\xi,\eta,z^*,\Omega) = -\overline{\Pi}(\eta)\overline{\overline{F}}_B^*(\xi,\Omega)\phi(\xi,\eta,z^*,\Omega) \tag{34}$$

So soil displacement in real domain can be expressed, by introducing auxiliary spatial coordinate $x_t^* = x^* - c^*\tau$, as

$$u_z(x_t^*,y^*,z^*) = \frac{1}{4\pi^2}\int_{-\infty}^{\infty}\int_{-\infty}^{\infty} -\overline{\Pi}(\eta)\overline{\overline{F}}_B^*(\xi,-\xi c^*)\phi(\xi,\eta,z^*,-\xi c^*)e^{i[\xi x_t^* + \eta y^*]}d\xi d\eta \tag{35}$$

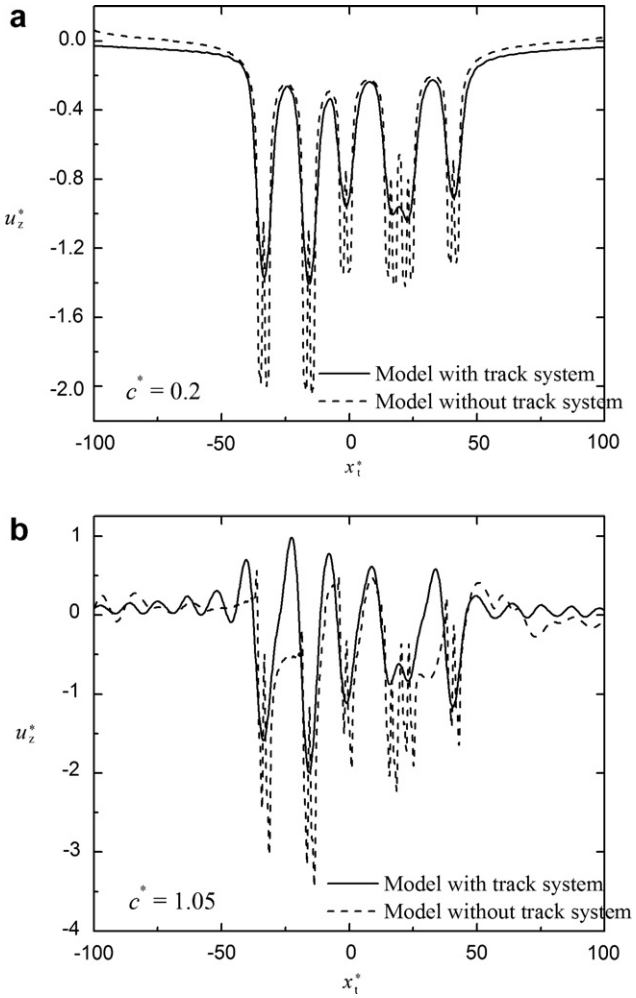

Fig. 4. Comparison between model with track system and model without track system: (a) $c^* = 0.2$, (b) $c^* = 1.05$.

2.3. Description of the train load

In deriving the ground vibration under train passage, a series of moving axle loads are formulated in view of the train geometry in Fig. 2. Here the model of Takemiya and Bian (2005) is employed:

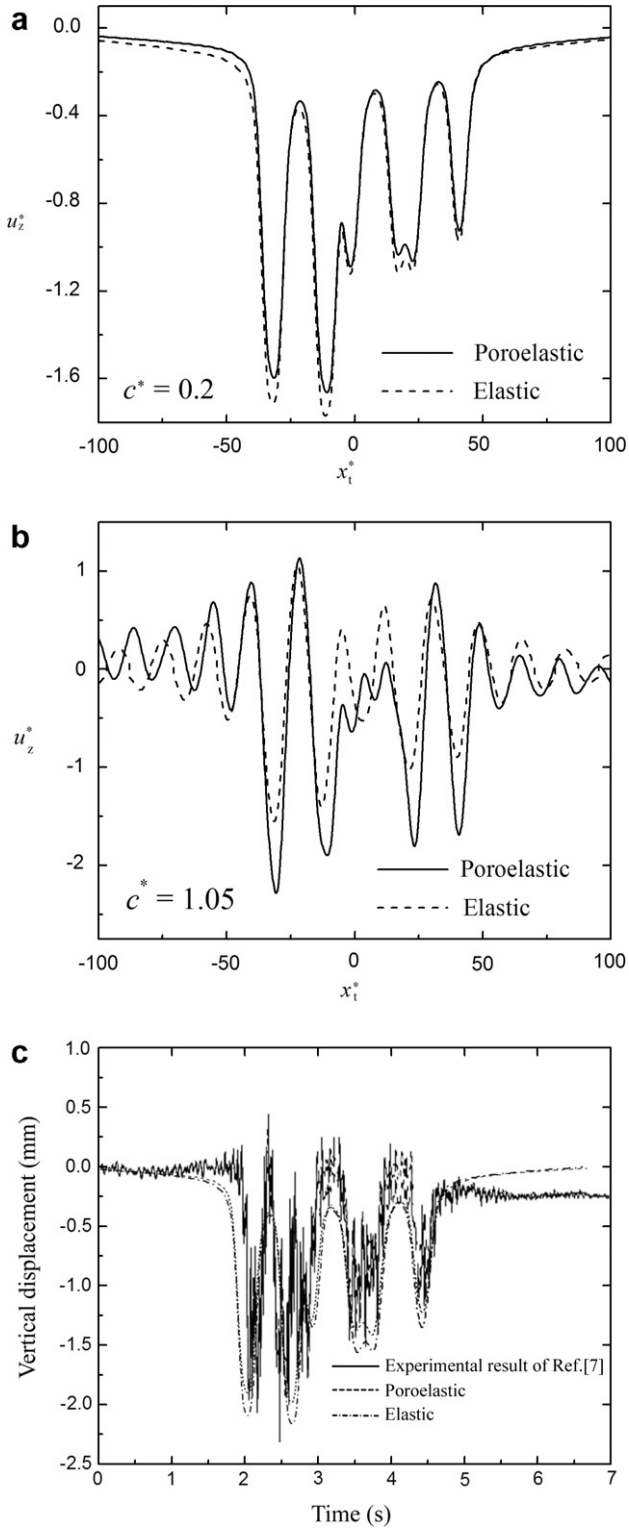

Fig. 5. Comparison between poroelastic medium and elastic medium: (a) $c^* = 0.2$, (b) $c^* = 1.05$, (c) $c^* = 0.2$ comparison with experimental result.

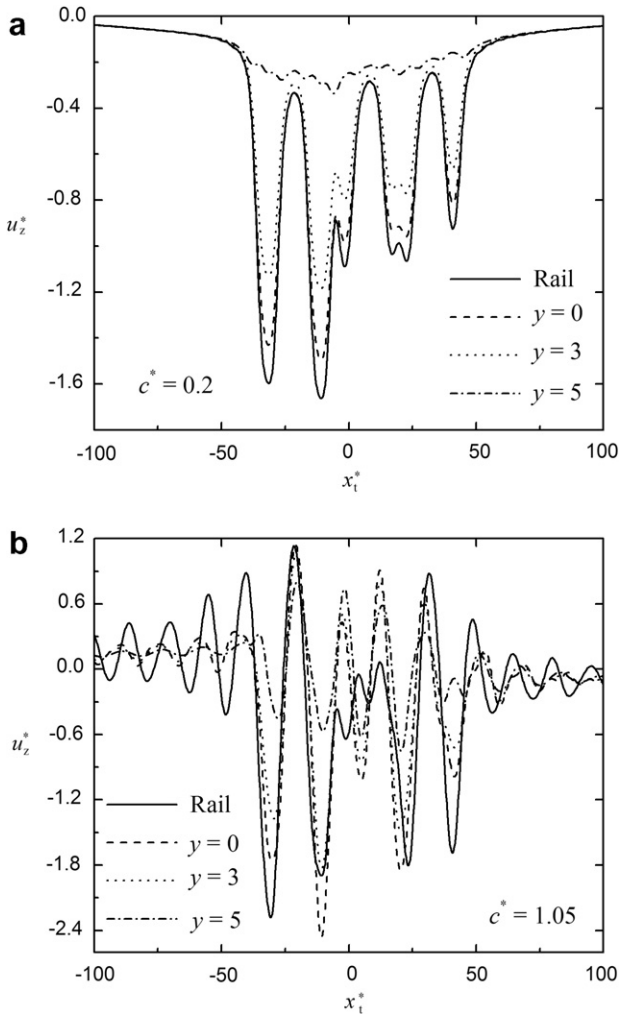

Fig. 6. Dimensionless vertical displacements varied with x_t^*: (a) $c^* = 0.2$, (b) $c^* = 1.05$.

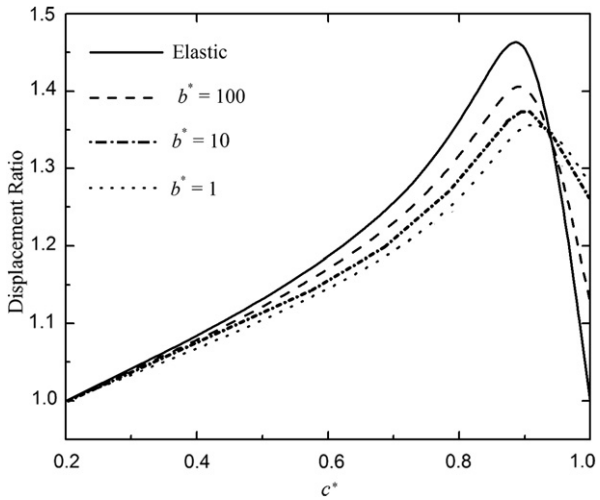

Fig. 7. Displacement ratio variation with c^*.

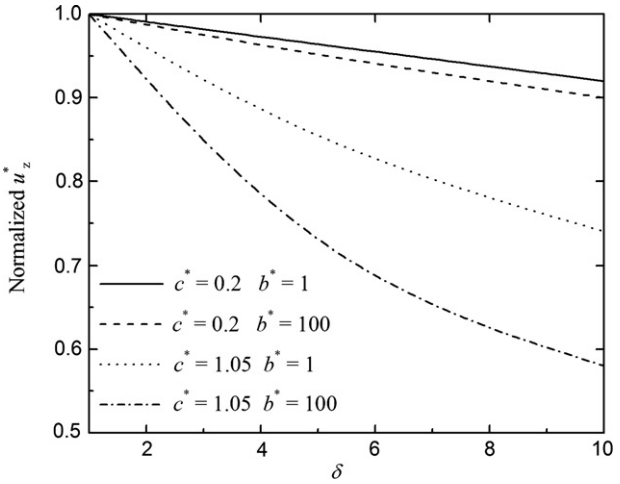

Fig. 8. Effect of δ on vertical rail displacement under different c^* and b^*.

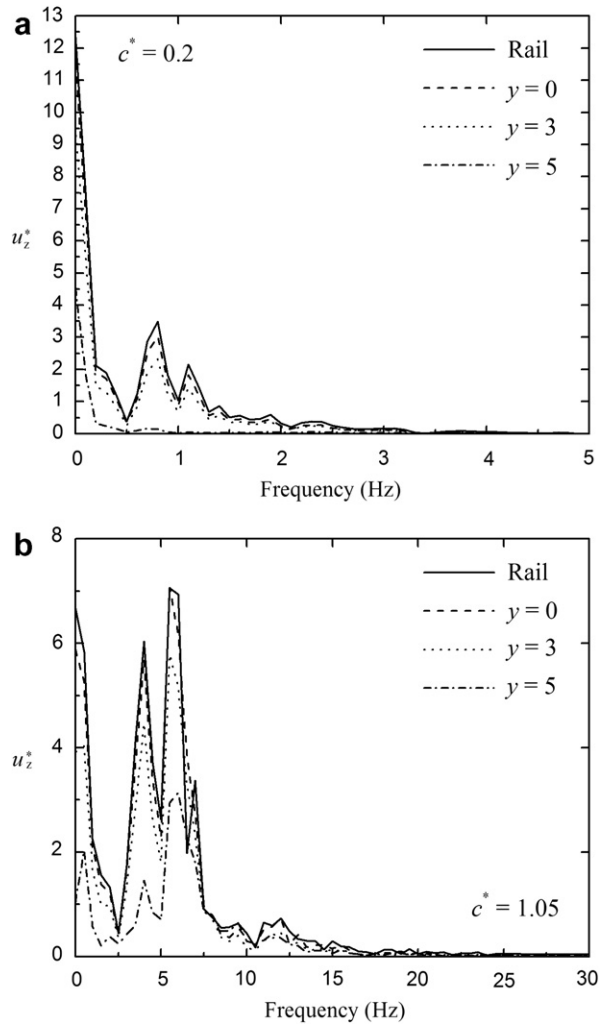

Fig. 9. Fourier amplitudes of displacements: (a) $c^* = 0.2$, (b) $c^* = 1.05$.

$$p_n^{xt}(\xi,\Omega) = 2\pi\delta(c^*\xi - \Omega)\chi_{N_T}(\xi) \tag{36}$$

where

$$\chi_{N_T}(\xi) = \sum_{n=1}^{N_T}\Big\{P^*_{Eng}(1 + e^{-ia_t^*\xi} + e^{-i(a_t^*+b_t^*)\xi} + e^{-i(2a_t^*+b_t^*)\xi}) + P^*_{Wag}(1 + e^{-ia_t^*\xi} + e^{-i(a_t^*+b_t^*)\xi} + e^{-i(2a_t^*+b_t^*)\xi})e^{-i(n-1)L^*_{Wag}\xi}e^{-i(d_t^*+L^*_{Eng})\xi}\Big\}e^{-iL^*_{Dis}\xi} \tag{37}$$

in which, $P^*_{Eng} = P_{Eng}/\mu a^2$ and $P^*_{Wag} = P_{Wag}/\mu a^2$ are the dimensionless axle loads of the engines and the carriages respectively, N_T is the number of the carriages, $L^*_{Eng} = L_{Eng}/a$ and $L^*_{Wag} = L_{Wag}/a$ are the dimensionless engine length and carriage length respectively, $a_t^* = a_t/a$ is the dimensionless distance between the first and second axles of a carriage, $b_t^* = b_t/a$ is the dimensionless distance between the second and third axles of a carriage. $d_t^* = d_t/a$ is the dimensionless distance between the first axle of a carriage and the end of the former carriage, $L^*_{Dis} = L_{Dis}/a$ is the dimensionless distance of the train and the observation point. The parameters of the train are given in Table 1 which are from Takemiya and Bian (2005).

3. Numerical analysis results and discussion

In this study, fast Fourier transform (FFT) was used to perform the inverse transform with respect to ξ and η. To compute the inverse transform accurately with a discrete transform, the integrals must be truncated at sufficiently high values to

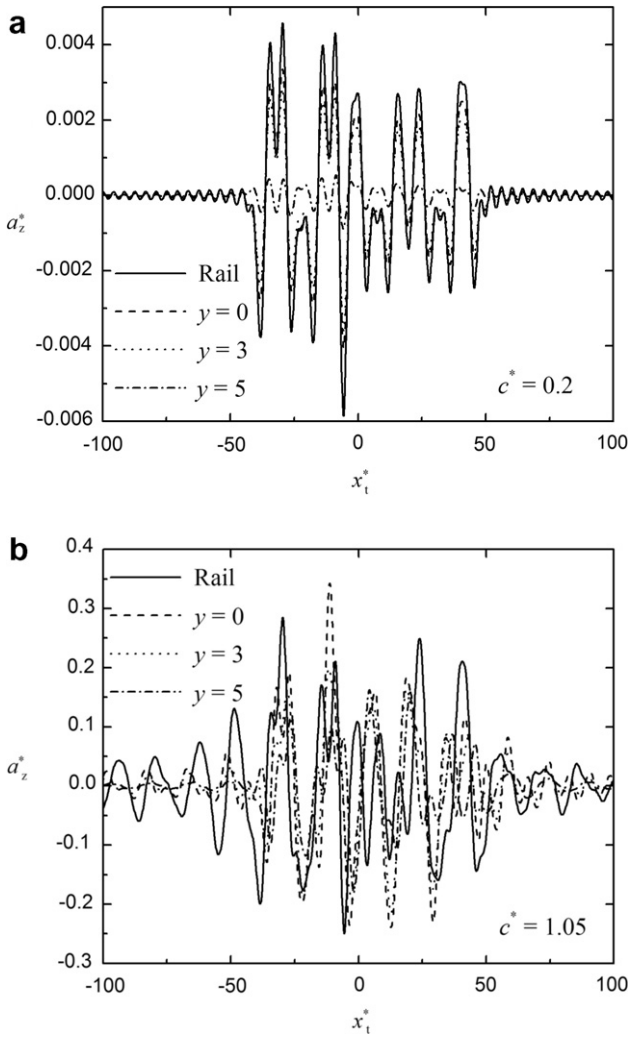

Fig. 10. Dimensionless vertical accelerations varied with x_t^*: (a) $c^* = 0.2$, (b) $c^* = 1.05$.

avoid distortion of the results, while the mesh of the calculated functions must be fine enough to represent well the details of the functions. According to the analysis of Takemiya and Bian (2005), an FFT algorithm is employed with a grid of 1024×1024 points over a range of $-4 < \xi < 4$ and $-4 < \eta < 4$ to satisfy both these requirements. For the cases of transonic speeds, the pole of the integrands can be shifted off the real axis ξ and η by introducing material attenuation. The material damping can be taken into account through use of complex Lame's constants, i.e. $\lambda^c = \lambda^*(1 + 2i\beta)$ and $\mu^c = \mu^*(1 + 2i\beta)$, where β denotes the hysteretic damping ratio.

The normalized displacements, accelerations and excess pore water pressure in the following parts are defined as: $u_z^* = u_z(x_t^*, y^*, z^*)/P_{Eng}^*$, $a_z^* = a_z(x_t^*, y^*, z^*)/P_{Eng}^*$, $p^* = p(x_t^*, y^*, z^*)/P_{Eng}^*$, where $x_t^* = x^* - c^*\tau$. The track and soil properties are presented in Table 2, in which the soil parameters are from Jin (2004), and the track parameters are from Picoux and Le Houedec (2005).

3.1. Comparison between present works with Picoux

In order to verify the accuracy of the present procedure on further application to the train load, Fig. 3(a) compares the numerical result of rail vertical displacement given in Picoux and Le Houedec (2005) with that of the present work, in which V_R is defined as the Rayleigh-wave speed of the soil. The ballast is considered as the first layer of the ground as in Picoux and Le Houedec (2005). The dimensionless water density of the present work used in Fig. 3(a) is assumed to be a small value (10^{-3}) to degenerate the poroelastic soil into elastic soil, and other parameters of the track system and the ground are the same with those of Picoux and Le Houedec (2005). As can be seen, the results for the present work are in good agreement with the numerical result of Picoux and Le Houedec (2005).

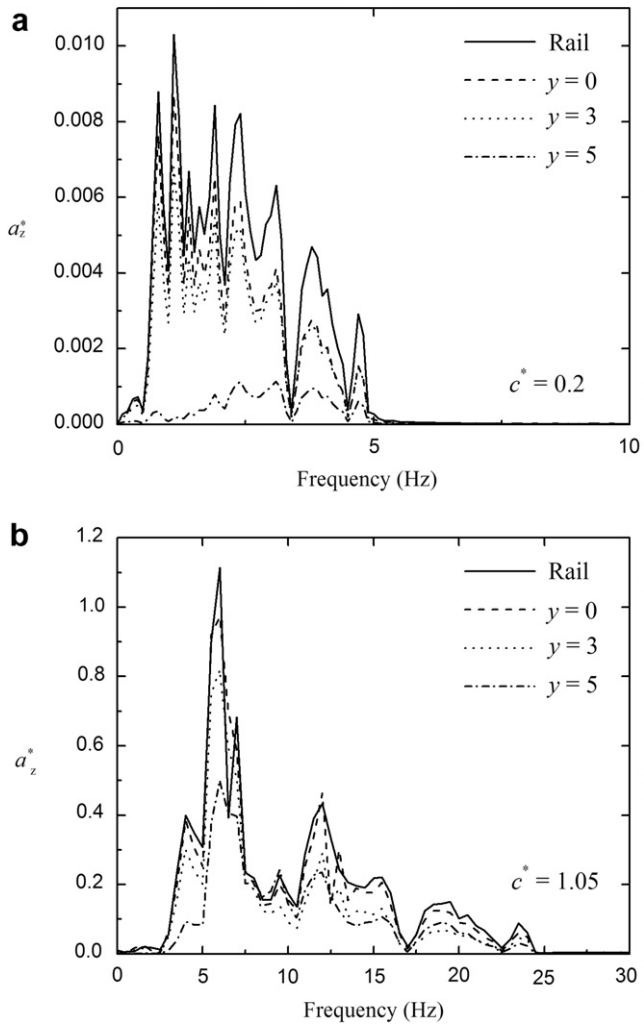

Fig. 11. Fourier amplitudes of accelerations: (a) $c^* = 0.2$, (b) $c^* = 1.05$.

3.2. Comparison between present works with Cai

For the sake of verifying the accuracy of the present method used for solving the Biot theory of the fully saturated poroelastic half-space, Fig. 3(b) compares the result of soil vertical displacement given in Cai et al. (2007) with that calculated by the method of the present work. The model of a fully saturated poroelastic half-space subjected to a moving rectangular load is employed, and the parameters for the calculation are the same for both method. It can be seen that the results for the present work and that of Cai et al. (2007) are in good agreement with each other.

3.3. Numerical results of present work

To limit the environmental vibration of the area on the train line-side, it particularly concerns the displacements and accelerations of the ground surface. In view of this, the displacement and acceleration responses of the ground surface are mainly discussed as follows, in which two carriages and one engine are taken into account for a train. The train is assumed to move at $c^* = 0.2$, which is far below the Rayleigh-wave velocity of the soil medium, and $c^* = 1.05$, which is beyond the Rayleigh-wave velocity of the soil medium.

3.3.1. Effect of the track system

The effect of the track system on soil dynamic response is shown in Fig. 4 in which soil displacement of the model with track system is compared with that of the model without track system. In the model without track system, the train loads directly act on the soil surface. It can be seen that the track system not only influence the amplitude of the soil displacement,

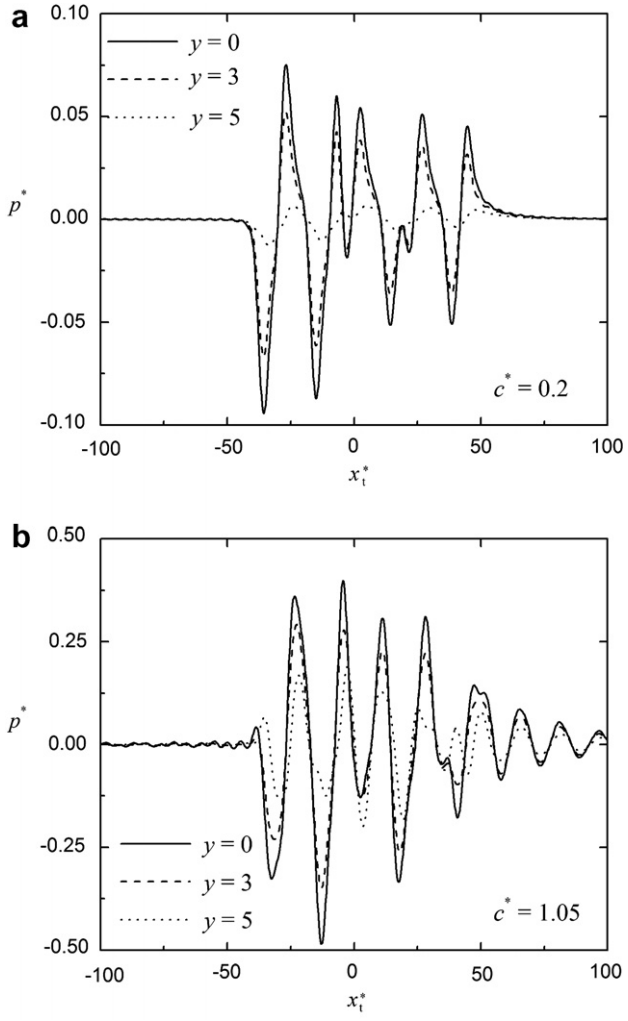

Fig. 12. Dimensionless excess pore water pressure varied with x_t^*: (a) $c^* = 0.2$, (b) $c^* = 1.05$.

but also redistribute the train load for both low and high train velocity. Therefore it is extremely important to consider the track system while studying the dynamic response to moving train load.

3.3.2. Displacement responses

Vertical displacements of elastic and poroelastic soil medium are compared in Fig. 5 under different train velocity. The vertical displacement of the poroelastic soil medium is smaller than that of the elastic soil medium for the low train velocity. However, for the high train velocity when $c^* = 1.05$, the vertical displacement of the poroelastic soil medium is larger than that of the elastic soil. The maximum amplitude difference is over 30%. This phenomenon is also given in Jin et al. (2004). The shape of the curves of the computed u_z^* of the two kinds of soil medium are in good agreement with each other of the low train velocity, but for the high train velocity, the results turn out to be quite different. Thus, dynamic responses analysis of some existing method considering the elastic soil medium is limited to cases with low train velocity.

Fig. 5(c) compares the numerical result of vertical displacement of the rail for the poroelastic half-space with the experimental result given in Picoux and Le Houedec (2005) and vertical displacement of the rail for elastic half-space for the same used computed parameters. The elastic half-space model used here is simulated by letting the dimensionless water density of the present work to be a small value (10^{-3}). At the same time, other parameters of poroelastic and elastic medium are the same with that given in Picoux and Le Houedec (2005). As can be seen, the results for the poroelastic half-space are in good agreement with the experimental result of Picoux and Le Houedec (2005). And it is clearly shown in Fig. 5(c) that the poroelastic model is closer to the experimental result than the elastic model. Therefore a fully saturated poroelastic soil model is a better choice to be used for the analysis of dynamic responses of the track-ground system.

Subjected to the train passages with the geometry of the axle loads shown in Fig. 2, the dimensionless vertical displacements of the rail and the ground are depicted in Fig. 6(a) and (b), respectively. If the train velocity is small, the deformation of

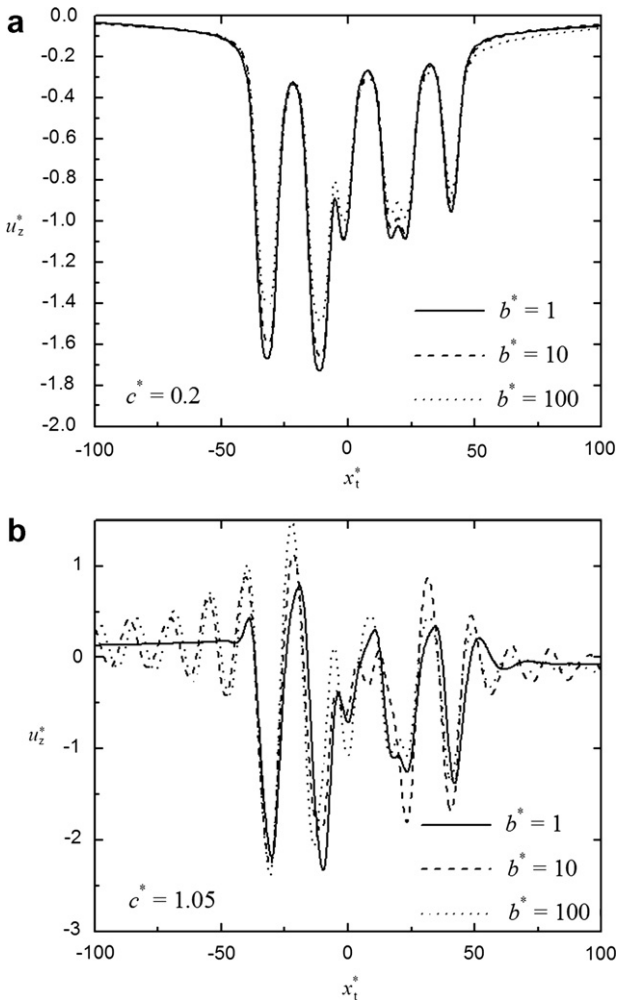

Fig. 13. Dimensionless rail vertical displacements varied with x_t^* under different b^*: (a) $c^* = 0.2$, (b) $c^* = 1.05$.

the rail and the ground surface just follow the layout of bogies. But if the train velocity is large, the effect of the inertial force is considerable so that the rail and the ground show significantly large dynamic responses. Fig. 6 also shows the effect of y^* on the vertical displacement responses of the ground. It was found that, bogies can heavily influence the displacement responses of the rail and the ground when $y^* = 0$. When $y^* = 5$ the contribution of the bogies are blurry and the dimensionless displacement decreases rapidly with the increasing of y^*.

As reported by Theodorakopoulos (2003), if the load velocity approaches the Rayleigh-wave velocity of the ground, as shown in Fig. 7, the displacement of the ground reaches a peak. In Fig. 7 the displacement ratio is defined as the ratio of the maximal dimensionless displacement to that of $c^* = 0.2$. A peak of displacement ratio appears in Fig. 7 if the train velocity approaches the Rayleigh-wave velocity of the ground ($c^* = 0.92$–0.93). The train velocity related to the maximal ground displacement of the poroelastic soil medium is larger than that of the elastic soil medium, and it increases with the decreasing of b^*. Here the fluid viscosity is assumed as a constant, and the variety of b^* denotes the variety of the intrinsic permeability of the soil medium. The case of $b^* = 100$ stands for soil with low intrinsic permeability such as clay, and $b^* = 1$ indicates soil with high intrinsic permeability such as sand.

The effect of rail rigidity on rail vertical displacement under different b^* is given in Fig. 8, in which, the normalized u_z^* is defined as ratio of u_z^* and u_z^* when $\delta = 1$. It is observed that the effect of δ on the rail vertical displacement is limited for the low train velocity, whether for high or low intrinsic permeability. However, when the train is moving at high velocity, δ has an effect on rail vertical displacement. Especially for soil which has a low intrinsic permeability such as clay, the rail vertical displacement decreases rapidly when δ increases. Thus, on soil with low intrinsic permeability such as clay, it is effective to increase the rigidity of the rails for the sake of reducing the ground vibration.

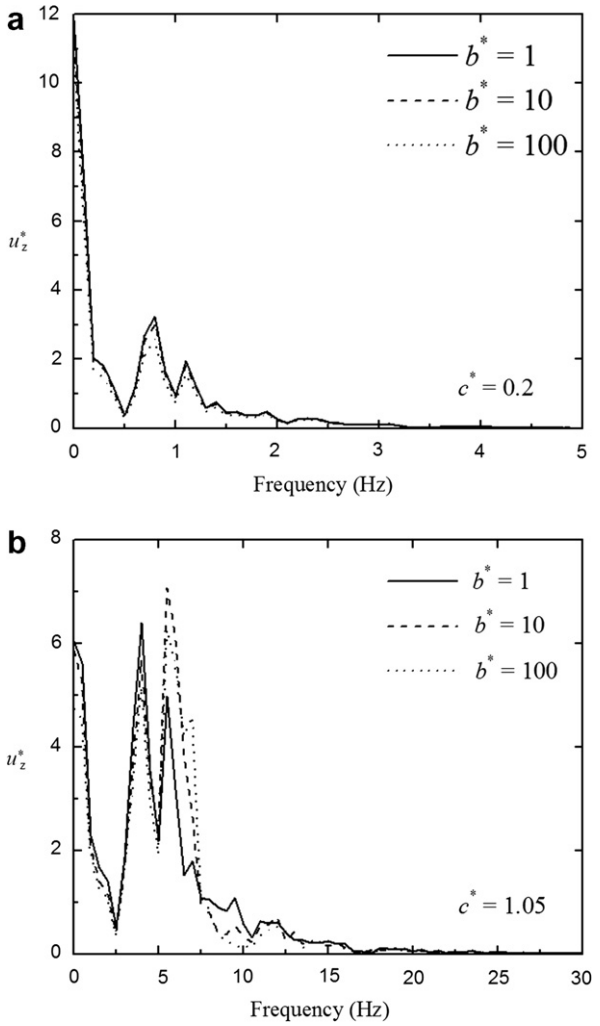

Fig. 14. Fourier amplitudes of rail displacements under different b^*: (a) $c^* = 0.2$, (b) $c^* = 1.05$.

To investigate the dynamic displacement responses of the system in frequency domain, their Fourier spectrums are given in Fig. 9. The quasi-static response due to the train weight is grouped in the frequency range lower than 0.2 Hz, and the peak around 0.7 Hz is associated with the train geometry against the train speed. The peaks in frequency range from 1 to 2 Hz are deemed to be originated from the bogie positioning. When $y^* = 5$, the main contributions to the ground displacement are from the train weight, and the responses associated with the train geometry are rather limited. In Fig. 9(b), the train velocity is assumed to be at $c^* = 1.05$, the subordinate peaks caused by the train geometry and bogies shift by the train speed ratio of 1.05/0.2 = 5.25. Corresponding to 0.7 Hz for the case of $c^* = 0.2$, the peak originate from the train geometry against the train speed shifted to 3.6 Hz. The contribution of the subordinate peaks is more amplified when train velocity increases. It is also observed that for high train velocity, the contribution of the ground response associated with the train geometry increases to an amplitude larger than the response associated with the train weight.

3.3.3. Acceleration responses

The dimensionless acceleration of the rail and the lines with distances $y^* = 0$, 3 and 5 away from the train line is plotted in Fig. 10, and their Fourier spectrums are given in Fig. 11, for different train velocities. If the train velocity is small ($c^* = 0.2$), peak values of the acceleration of the ground surface appear at the position on which axle loads of the train act. The influence of the bogies are both significant when $c^* = 0.2$ and 1.05. Frequencies of acceleration responses concentrate in several Hertz, for the given geometry of the train, when the time is converted to distance by multiplying the train speed. For the train velocity $c^* = 0.2$, the Fourier amplitudes are more dominated by frequencies 0.5–5 Hz than other frequencies. It is caused from the dynamic track interaction with the Rayleigh-wave propagation at the site. With the distance from the observation point increasing, the above predominant frequency still dominates the response there. For the case of $c^* = 1.05$, the dominate frequencies shift to a higher scale of 2.6–26 Hz by the speed ratio 5.25, and a predominant peak appears near 5 Hz. This is be-

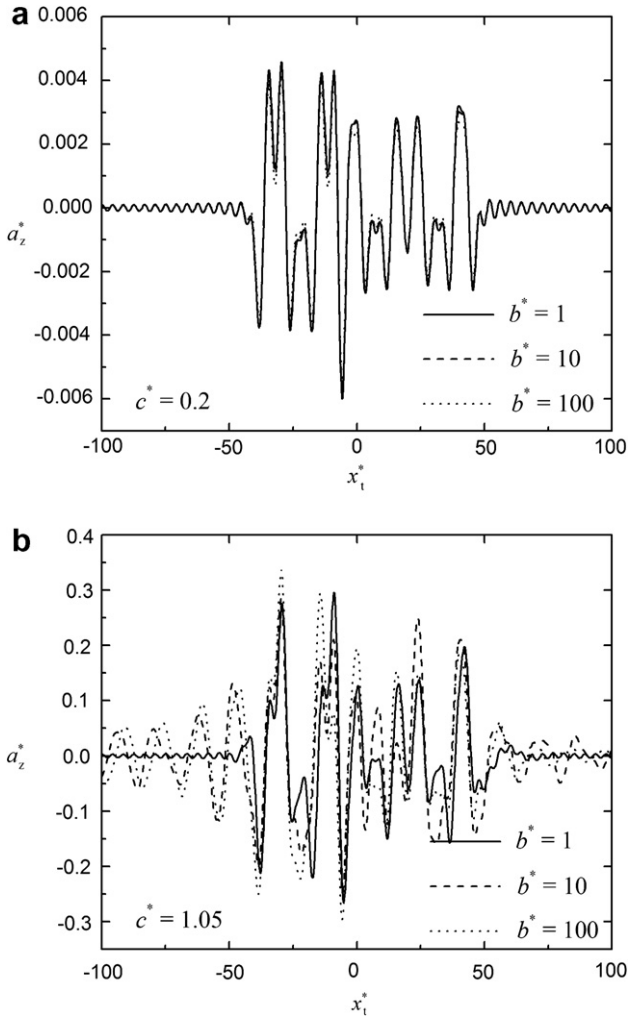

Fig. 15. Dimensionless rail vertical accelerations varied with x_t^* under different b^*: (a) $c^* = 0.2$, (b) $c^* = 1.05$.

cause that for high train velocity, the acceleration responses which caused by the distance of the second and the third axles loads of the train become significant.

3.3.4. Pore water pressure responses

It is important to study the excess pore water pressure of the soil medium during the train passages are passing, since it has considerable effect on settlement of the ground. The excess pore water pressure at $z^* = 1$, $y^* = 0$ is investigated as shown in Fig. 12. For the small train velocity of $c^* = 0.2$, peak values of the excess pore water pressure appear beneath the position that axle loads of the train acts on, but it is not so for the case of $c^* = 1.05$. In Fig. 12, the excess pore water pressure decreases significantly with the increasing of y^* both for $c^* = 0.2$ and 1.05.

3.3.5. Influence of the intrinsic permeability

One of the most crucial parameters that differentiate poroelastic medium from elastic medium is the intrinsic permeability of the soil which, proved in the following part, has significant influence on rail dynamic responses. Fig. 13 shows the influence of intrinsic permeability on rail displacement. For train velocity lower than R-wave velocity, say $c^* = 0.2$, the variety of b^* only influences the amplitude of the rail displacements. However for train velocity which is higher than R-wave velocity, the variety of b^* not only influences the amplitude of rail displacement, but changed the shapes of the displacement curve as well. In this case, significant vibration is observed when $b^* = 10$ and 100 which stand for soil with low intrinsic permeability such as clay. For $b^* = 1$ which indicates soil with high intrinsic permeability such as sand, the vibration is inconspicuous. This is because that, for soil with low intrinsic permeability, the effect of the coupling of the fluid and the soil skeleton is significant. The Fourier amplitudes of rail displacements are given in Fig. 14. As can be seen in Fig. 14(a), which presents the case of $c^* = 0.2$, the variety of b^* nearly influences rail displacement on the whole frequency range but the effect is limited. Never-

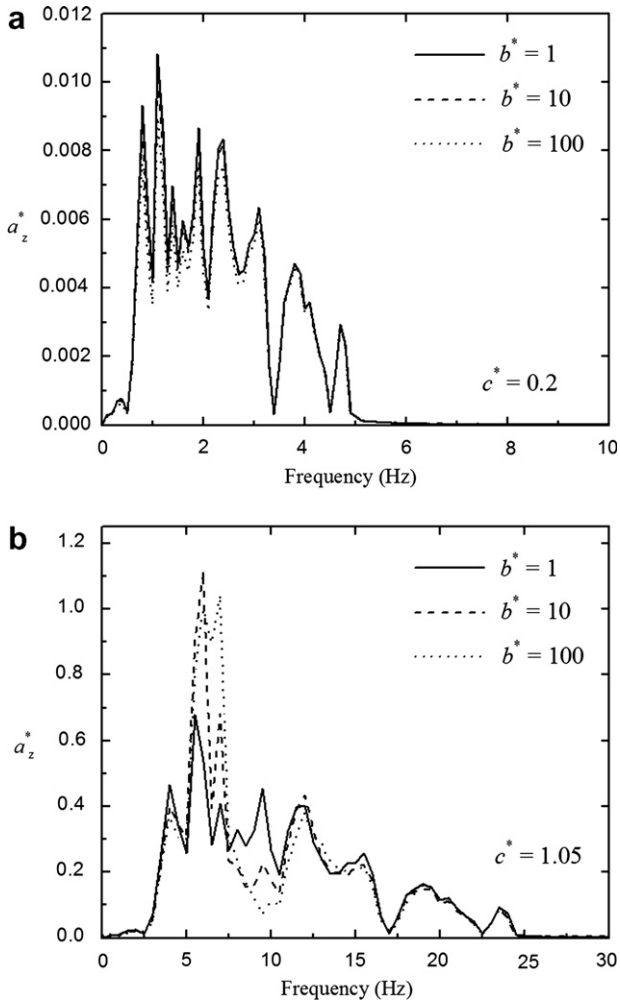

Fig. 16. Fourier amplitudes of rail accelerations under different b^*: (a) $c^* = 0.2$, (b) $c^* = 1.05$.

theless when $c^* = 1.05$ the effect of variety of b^* is obvious. When $b^* = 1$ the displacements originated from the train geometry distributed between 2.5 and 15 Hz, and when $b^* = 10$ and 100, they tend to gather between 5 and 7.5 Hz, namely, when b^* increases the displacement distributed between 2.5 and 5 Hz and 7.5 and 15 Hz decreases and the displacement distributed between 5 and 7.5 Hz increases significantly. The explanation of the phenomenon is the viscous effect of the fluid in the soil.

The influence of b^* on rail acceleration and Fourier spectrums of rail acceleration are presented in Figs. 15 and 16, respectively. The same as in the case of Fig. 13, for low train velocity b^* only influences the amplitude of the rail displacements and the effect is limited. However in the case of high train velocity, significant vibration is observed when $b^* = 10$ and 100. For $b^* = 1$ the vibration is inconspicuous. It is shown in Fig. 16(a), which presents the case of $c^* = 0.2$, the whole frequency range is influenced by b^* but the effect is limited. However when $c^* = 1.05$ the effect of variety of b^* is obvious. When $b^* = 10$, the acceleration originated from the train geometry tend to gather between 5 and 7.5 Hz, which is the same as in the case of displacement. When b^* increases the acceleration distributed between 2.5 and 5 Hz and 7.5 and 17.5 Hz decreases and the acceleration distributed between 5 and 7.5 Hz increases significantly.

Fig. 17(a) and (b) give the excess pore water pressure at different depth when $y^* = 0$ for $c^* = 0.2$ and 1.05, respectively. It is observed that the excess pore water pressure increases rapidly with the increasing of b^*. The maximal excess pore water pressure appears at about $z^* = 2$–6, and for higher value of b^* the peak value appears in the shallower layer of the soil. For the low permeable soil medium such as the soft clay, the high speed train will induce high dynamic excess pore water pressure in the ground which can soften the soft clay and result in large settlement of the ground. But it only needs to treat the soft ground in several meters because the effect of the train on the excess pore water pressure of deeper soil medium is limited. The influence of rail rigidity on excess pore water pressure under different b^* is presented in Fig. 18, in which, the normalized p^* is defined as ratio of p^* and p^* when $\delta = 1$. It is observed that, for the low train velocity, the effect of δ on the excess

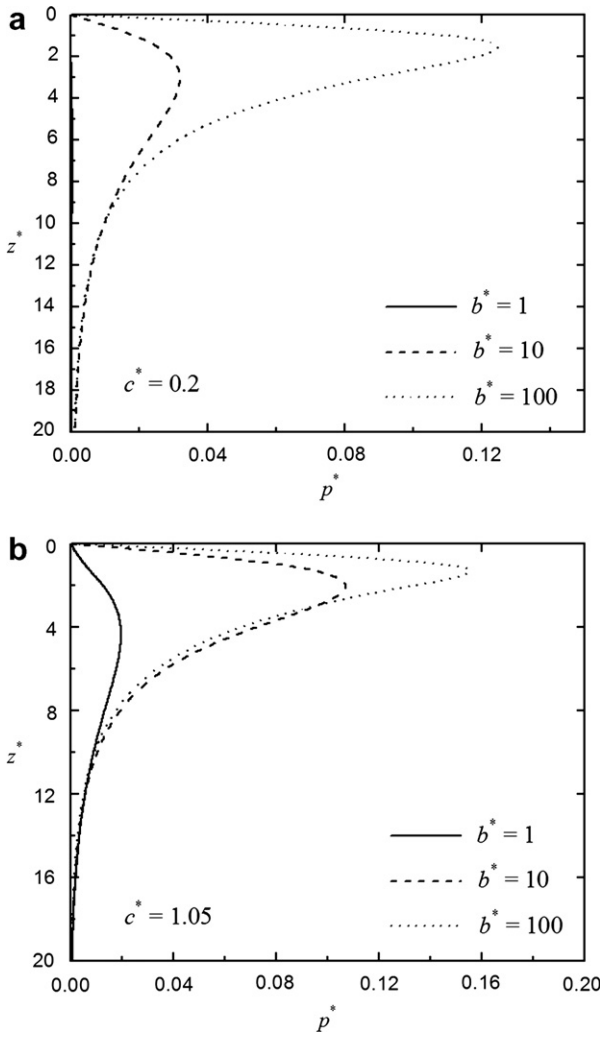

Fig. 17. Pore water pressure variation with z under different b^*: (a) $c^* = 0.2$, (b) $c^* = 1.05$.

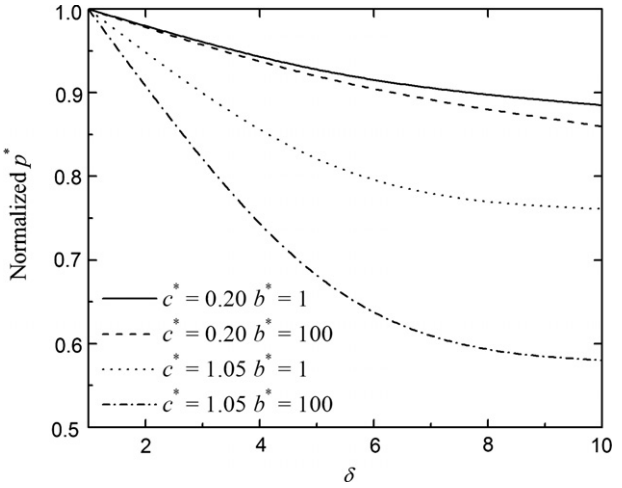

Fig. 18. Effect of δ on excess pore water pressure under different c^* and b^*.

pore water pressure is limited, whether for high or low intrinsic permeability. But if the train velocity is high, δ has obvious effect on excess pore water pressure. Especially for soil which has a low intrinsic permeability such as clay, the excess pore water pressure decreases rapidly when δ increases.

4. Conclusions

In this work, a track and poroelastic half-space soil medium subjected to moving train passages are investigated with due consideration to dynamic interaction between a track system comprising continuous rails, sleepers and ballast, and the underlying poroelastic half-space ground. The moving train load is simulated by a series of moving axle loads formulated in views of the train geometry. The double Fourier transform is employed, and the governing equations of motion are solved analytically in the frequency-wave-number domain. The time domain responses are evaluated by the inverse Fourier transform computation for a certain train speed. Computed results of the proposed model are compared with those of existing methods. The following conclusions can be drawn from the numerical studies:

1. The effect of δ on rail vertical displacement is limited for low train velocity. However for high train velocity, δ has obvious effect on rail vertical displacement. Especially for soil with low intrinsic permeability, it is effective to increase the rigidity of the rails for the sake of reducing the ground vibration.
2. In the time domain: when the train speed is low, the deformation of the soil just follows the layout of bogies and the vertical displacement of the poroelastic soil medium is smaller than that of the elastic soil medium. When the train speed is high, the vertical displacement of the poroelastic soil medium is larger than that of the elastic soil. The variety of b^* only influences the amplitude of the rail displacements and acceleration for train velocity lower than R-wave speed. For train velocity which is higher than R-wave speed, the variety of b^* not only influences the amplitude of rail displacement and acceleration, but changed the shapes of the displacement and acceleration curves as well. Significant vibration is observed for rail responses when $b^* = 10$ and 100 which stand for soil with low intrinsic permeability such as clay. For $b^* = 1$ which indicates soil with high intrinsic permeability such as sand, the vibration is inconspicuous.
3. In the frequency domain: the whole frequency range is influenced by b^* for both rail displacement and acceleration when $c^* = 0.2$ but the effect is limited. However when $c^* = 1.05$ the effect of variety of b^* is obvious. When $b^* = 10$ and 100, the displacement and acceleration originated from the train geometry tend to gather between 5 and 7.5 Hz. The displacement and acceleration distributed between 2.5 and 5 and 7.5 and 17.5 Hz decreases and those between 5 and 7.5 Hz increases significantly as b^* increases.
4. Pore water pressure increases rapidly, and a sharp peaks appear clearly at the moment when the axle loads move over a focused point. For the low train velocity, the effect of δon the excess pore water pressure is limited, whether for sand or soft clay. If the train velocity is high, δhas an effect on excess pore water pressure. Especially for soil which has a low intrinsic permeability such as clay, the excess pore water pressure decreases rapidly when δ increases.

Acknowledgments

The project is supported by National Natural Science Foundation of China through Grand No. 50778136. The constructive comments from the two anonymous referees are highly appreciated.

References

Biot, M.A., 1956. Theory of propagation of elastic waves in a fluid-saturated porous solid. Part I: Low-frequency range. Part II: High-frequency range. Journal of the Acoustical Society of America 28 (4), 168–191.

Burke, M., Kingsbury, H.B., 1984. Response of poroelastic layers to moving loads. International Journal of Solids and Structures 20 (5), 499–511.

Cai, Y.Q., Sun, H.L., Xu, C.J., 2007. Steady state responses of poroelastic half-space soil medium to a moving rectangular load. International Journal of Solids and Structures 44, 7183–7196.

Jin, B., 2004. Dynamic response of a poroelastic half space generated by high speed load. Chinese Quarterly of Mechanics 25 (2), 168–174.

Jin, B., Yue, Z.Q., Tham, L.G., 2004. Stresses and excess pore pressure induced in saturated poroelastic half-space by moving line load. Soil Dynamics and Earthquake Engineering 24, 25–33.

Kargarnovin, M.H., Younesian, D., 2004. Dynamics of Timoshenko beams on Pasternak foundation under moving load. Mechanics Research Communications 31 (6), 713–723.

Kargarnovin, M.H., Yournesian, D., Thompson, D.J., et al, 2005. Response of beams on nonlinear viscoelastic foundations to harmonic moving loads. Computers and Structures 83 (23–24), 1865–1877.

Kennedy, T.C., Herrmann, G., 1973a. Moving load on a fluid–solid interface: subsonic and intersonic regimes. Journal of Applied Mechanics 40, 885–890.

Kennedy, T.C., Herrmann, G., 1973b. Moving load on a fluid–solid interface: supersonic regimes. Journal of Applied Mechanics 40, 137–142.

Kim, S.M., 2004. Vibration and stability of axial loads beams on elastic foundation under moving harmonic loads. Engineering Structures 26 (1), 95–105.

Kim, S.M., 2006. Vibration and dynamic buckling of shear beam-columns on elastic foundation under moving harmonic loads. International Journal of Solids and Structures 43 (3–4), 393–412.

Picoux, B., Le Houedec, D., 2005. Diagnosis and prediction of vibration from railway trains. Soil Dynamics and Earthquake Engineering 25 (12), 905–921.

Sheng, X., Jones, C.J.C., Petyt, M., 1999. Ground vibration generated by a harmonic load acting on a railway track. Journal of Sound and Vibration 228 (1), 3–28.

Siddharthan, R., Zafir, Z., Norris, G.M., 1993. Moving load response of layered soil. Part I: Formulation. Part II: Verification and application. Journal of Engineering Mechanics 119 (10), 2052–2089.

Suiker, A.S.J., Chang, C.S., Borst, R.D., et al, 1999. Surface waves in a stratified half space with enhanced continuum properties. Part 1: Formulation of the boundary value problem. European Journal of Mechanics A: Solids 18, 749–768.

Takemiya, H., Bian, X.C., 2005. Substructure simulation of inhomogeneous track and layered ground dynamic interaction under train passage. Journal of Engineering Mechanics 131 (7), 699–711.

Theodorakopoulos, D.D., 2003. Dynamic analysis of a poroelastic half-plane soil medium under moving loads. Soil Dynamics and Earthquake Engineering 23 (7), 521–533.

Theodorakopoulos, D.D., Chassiakos, A.P., Beskos, D.E., 2004. Dynamic effects of moving load on a poroelastic soil medium by an approximate method. International Journal of Solids and Structures 41 (7), 1801–1822.

Vostroukhov, A.V., Metrikine, A.V., 2003. Periodically supported beam on a visco-elastic layer as a model for dynamic analysis of a high-speed railway track. International Journal of Solids and Structures 40 (21), 5723–5752.